X-646-72-405

SEASONAL AND ALTITUDE VARIATIONS IN FIELD-ALIGNED PRECIPITATION OCCURRENCE

F. W. BERKO

OCTOBER 1972

GODDARD SPACE FLIGHT CENTER
GREENBELT, MARYLAND

SEASONAL AND ALTITUDE VARIATIONS IN FIELD-ALIGNED PRECIPITATION OCCURRENCE

By

F. W. Berko

NASA-Goddard Space Flight Center
Greenbelt, Maryland 20771

October 1972

SEASONAL AND ALTITUDE VARIATIONS IN FIELD-ALIGNED PRECIPITATION OCCURRENCE

SUMMARY

Data from more than 7500 orbits of the polar-orbiting satellite OGO-4 have been analyzed to determine the existence of seasonal, altitude, or universal time differences in the occurrence of field-aligned electrons. Unexpected variations in frequency of occurrence have been found at different altitudes and in different seasons. In particular, the probability of observing this phenomenon at high latitudes was found to be greatest in the winter months at the highest altitudes attained by OGO-4. A localized parallel electric field acceleration mechanism is presented which could account for the particle observations.

INTRODUCTION

Field-aligned particles and field-aligned currents have been measured under a variety of magnetic conditions and at many different local times and altitudes. Observations of these phenomena at sounding rocket altitudes have been reported recently by Cloutier et al. (1970), Choy et al. (1971), Whalen and McDiarmid (1972) and many others. Satellite observations have been reported by Hoffman and Evans (1968), Zmuda et al. (1966, 1967, 1970), Ackerson and Frank (1972), Haerendel et al. (1971) and others at altitudes ranging from several hundred kilometers to 14 R_E.

Using data from the OGO-4 Auroral Particles Experiment (Hoffman and Evans, 1967), the spatial distribution, spectral characteristics and relationships to visual aurora of 2.3 keV field-aligned electron precipitation were recently determined by Berko (1972). Electron precipitation data from OGO-4 are available for an 18-month period (July, 1967, through

December, 1968) at satellite altitudes ranging from about 400 km to 925 km, at all magnetic local times (MLT), and invariant latitudes (Λ) primarily greater than 60°, and under all magnetic conditions. High-latitude field-aligned 2.3 keV electron precipitation was found to occur primarily in a roughly oval-shaped region, with the greatest number of field-aligned events observed in the interval $67.5^{\circ} \leq \Lambda \leq 72.5^{\circ}$ and 22 hours $\leq$ MLT $\leq$ 01 hour. Field-aligned events were defined as one-second periods of electron precipitation satisfying the following criteria: (1) the average near-0° pitch angle (α) 2.3 keV flux was at least 2×10^7 electrons/cm^2-sec-ster-keV, and (2) the ratio of $\alpha=0^{\circ}$ 2.3 keV flux to $\alpha=60^{\circ}$ 2.3 keV flux was greater than $1 + \Delta$, where Δ, the combined statistical uncertainty in the ratio, is a function of the particle counting rates at $\alpha=0^{\circ}$ and $\alpha=60^{\circ}$ (N_0 and N_{60}):

$$\Delta = (1/\sqrt{N_0} + 1 / \sqrt{N_{60}}) / \sqrt{2}.$$

In previous work (Berko, 1972), only events with $\Delta \geq 0.53$ were considered to have met the criteria; in this study, periods with Δ as low as 0.09 have been included, greatly increasing the quantity of data being considered. This letter investigates the universal time, seasonal, and altitude variations in the occurrence of these events, and proposes an acceleration mechanism to explain the observations.

UNIVERSAL TIME AND SEASONAL EFFECTS

The effects, if any, of universal time (UT) on field-aligned precipitation are not obvious or straightforward. As indicated in Figure 1, there is an apparent peak in the percent of field-aligned events (at all

Λ's and MLT's) per hour UT (normalized to account for uneven sampling in UT) at 9 to 10 hours, but the percent of events fluctuates too much from hour to hour to make this peak meaningful. If one considers only precipitation in the interval $67.5^{o} \leq \Lambda \leq 75^{o}$ and 22 hours $\leq$ MLT $\leq$ 1 hour, the percent of field-aligned events appears to be peaked in the UT intervals 9-10, 12-14, and 20-21 hours. Thus, even the precipitation in the region of maximum field-aligned events (Berko, 1972) shows no clear UT dependence.

Seasonal effects do seem to influence the occurrence of field-aligned precipitation, and may be associated with possible UT effects. After normalizing the percent of field-aligned events in each season to account for uneven seasonal sampling of precipitation, a definite winter peak appears. As indicated in Table 1, almost 40% of the seasonally normalized field-aligned events occurred during the winter season, while only 12.6% were detected in the summer. Even taking into account that 24.3% of all winter precipitation events occurred in the 22 hour to 01 hour MLT interval, but only 12.7% of the summer events were within this local time sector, the MLT interval in which more than half of all field-aligned precipitation was observed, there is still a distinct peak in the winter months.

The combined seasonal and UT effects on field-aligned precipitation are illustrated in Figure 2 for the winter and summer months. During the winter months, when the high-latitude northern hemisphere is receiving only minimal amounts of normally-incident solar radiation, most of the field-aligned precipitation was observed between 9 and 15 hours UT. In

the summer months, when solar heating is much greater in the northern hemisphere, almost 50% of the field-aligned events were observed between 15 and 21 hours UT. There are no simple explanations for these seasonal-UT variations, but the introduction of altitude as an additional parameter leads to a systematic seasonal dependence, as will be discussed below.

VARIATIONS WITH ALTITUDE AND SEASON

The variation in the number of field-aligned events with satellite altitude is an effect which appears to be closely associated with seasonal effects. The percentages of field-aligned events and of the total number of 2.3 keV precipitation events in each season at the highest and lowest altitudes attained by OGO-4 are listed in Table 2, as well as the totals for all seasons. From the tabulated values, based on data collected under approximately equal periods of quiet and disturbed magnetic activity in each season, we see that in the winter and autumn months, field-aligned precipitation occurred with much higher probability at altitudes greater than 800 km than at low altitudes. In contrast, the probabilities are about equal in the spring and summer months at high and low altitudes.

As shown in Figure 3, the probability of precipitation being field-aligned, considering data collected at all local times, and at similar samplings of magnetic disturbances, is about equal at the high and low OGO-4 altitudes during the summer, but is almost four times higher at altitudes > 800 km than altitudes < 500 km in the winter. In the region of highest occurrence of field-aligned precipitation (22 hours to 01 hour MLT), the probabilities below 500 km are about equal in winter and summer,

but above 800 km, the winter season probability is four times higher than the summer value (Figure 4). Again, these two sets of data were obtained under roughly equal periods of magnetically quiet and disturbed conditions.

IONOSPHERIC SCATTERING AND CONDUCTIVITY

Since both the altitude and universal time variations are associated with seasonal differences, it is reasonable to seek some relationship between them. Solar heating of the ionosphere increases its conductivity and raises its density at higher altitudes. Only the very low density upper high latitude ionosphere is appreciably sunlit during the winter and for most of autumn. During the spring and summer months, the northern hemisphere ionosphere expands in altitude due to heating of its lower layers by fairly direct sunlight, and the plasma density of the lower ionosphere increases due to electron heating (Coroniti and Kennel, 1972). The degree to which ionospheric scattering and conductivity changes might influence the altitude differences observed in the occurrence of field-aligned precipitation can be readily determined.

The angular spreading, or "de-focusing", of a beam of 2.3 keV field-aligned electrons due to ionospheric scattering at high altitudes can be calculated fairly easily. Taylor et al. (1971) have reported high latitude H^+ number densities of 2-4 x $10^1/cm^3$ at 500-600 km altitudes and 3-4 x $10^2/cm^3$ at 800-900 km altitudes measured by OGO-4 at the autumnal equinox. Using the empirical relation given by Fermi (1950) for the angular spreading of a beam of electrons due to scattering, and normalizing the values of Taylor and co-workers to sea level atmospheric

density, one computes that the angular spreading of an initially anisotropic (i.e. field-aligned) beam of 2.3 keV electrons due to upper ionospheric scattering is less than $\sim 2 \times 10^{-7}$ degrees at altitudes greater than 500 km. Thus, electron scattering in the ionosphere cannot account for an enhanced number of field-aligned precipitating electrons at higher altitudes than at lower altitudes.

Ionospheric conductivities are functions of density and collision frequency. As shown by Hanson (1965), the ionospheric conductivity in the direction of the magnetic field, often referred to as the ordinary or parallel conductivity, is given by:

$$\sigma_{\parallel} \cong n\, e^2 \left[\frac{1}{m_e \nu_e} + \frac{1}{m_i \nu_i} \right] ,$$

where n is the electron (or ion) number density, ν_e and ν_i are electron and ion collision frequencies, and m_e and m_i are the electron and ion masses. Using 1.6×10^{-20} emu for the electron charge, Hanson calculates that the parallel conductivity (in sunlight) varies from $\sim 5 \times 10^{-10}$ abmho/cm at 500 km to $\sim 7.5 \times 10^{-10}$ abmho/cm at 900 km. Nighttime values were found to be $\sim 3 \times 10^{-10}$ abmho/cm at 500 km and $\sim 8 \times 10^{-10}$ abmho/cm at 900 km. The nighttime values should correspond roughly to a winter season ionosphere, while daytime values should approximate summer conditions. Neither Pederson nor Hall conductivities are usually appreciable at altitudes greater than $\sim$ 300 km (Hanson, 1965). Although the high altitude winter (nighttime) conductivity is more than twice that at low altitudes, this difference cannot explain the enhanced winter high altitude occurrence of field-aligned precipitation, since if the precipitation

were field-aligned at 900 km, the conductivity would not prevent it from remaining so at 500 km. Thus, sunlight ionospheric conductivity enhancement is not able to explain the higher probability of observing field-aligned precipitation at high altitudes during the winter months.

PARALLEL ELECTRIC FIELDS

Magnetic field lines penetrating into the upper ionosphere cannot carry unlimited amounts of parallel current. Kindel and Kennel (1971) have shown that when fluxes of charged particles exceed certain threshold values, (comparable to those typically measured by OGO-4 during bursts of field-aligned electrons), the ionosphere is unstable to plasma wave growth, and electrostatic-wave instabilities will be generated in the topside ionosphere. The non-linear development of current driven instabilities leads to the appearance of 'anomalous' parallel resistivities in the ionosphere, and thus to the establishment of (localized) parallel electric fields. Kindel and Kennel show that the thresholds of current necessary to drive the ion-cyclotron or ion-acoustic instabilities responsible for the anomalous resistivities are proportional to the ionospheric density; i.e., the denser the ionosphere, the higher the critical current necessary to trigger an instability.

In examining the relationship of parallel electric fields to the observations of field-aligned electrons, certain physical constraints must be considered. Charged particles moving in the earth's magnetic field undergo motion governed by adiabatic constants of motion (Roederer, 1967). The first adiabatic invariant, μ, the magnetic moment, is defined by

$$\mu = \frac{W_\perp}{B} = \frac{W \sin^2\alpha}{B} = \text{constant}, \qquad (1)$$

where W is the energy of the particle, α is the pitch angle, and B is the magnetic field strength. For a particle moving between an initial and final location, equation 1 can be written in the equivalent form

$$\frac{W_i \sin^2 \alpha_i}{B_i} = \frac{W_f \sin^2 \alpha_f}{B_f} \qquad (2)$$

In addition to conserving the magnetic moment, particles moving through an electric potential V extending over a finite region of space must also satisfy energy conservation

$$W_f = W_i + eV, \qquad (3)$$

where W_i is the initial kinetic energy and W_f is the kinetic energy of the particle with charge e after having passed through an electric field region with potential V.

Electrons traversing a region of parallel electric field will be accelerated by the amount given in equation 3. If the energy of the electron increases faster than the magnetic field (to conserve μ), then from equation 2 it follows that the pitch angle distribution at B_f (where the electron exits the accelerating field) will have an upper maximum less than 90^o.

Assuming that the electrons were fairly isotropic when they entered the $E_{//}$, then the pitch angle cutoff under the above conditions at B_f is given by

$$\sin^2 \alpha_f^{max} = \frac{B_f W_i}{B_i W_f} < 1 \qquad (4)$$

Thus, the width of the pitch angle distribution at B_f will decrease with increasing ratio of energy increase to magnetic field increase between B_i and B_f. This parallel electric field acceleration process is therefore a focusing mechanism, leading to a pitch angle distribution cut-off at progressively smaller angles, i.e. eventually a field-aligned pitch angle distribution. Indeed, Chamberlain (1969) has noted that particles accelerated through relatively large potentials would preferentially emerge with small pitch angles.

Liouville's theorem tells us that the ratio of the differential directional flux at energy W, j(W), to the energy W is a constant along the particle's trajectory. Thus, we have the additional condition that

$$\frac{j_i\ (W_i,B_i)}{W_i} = \frac{j_f\ (W_f,B_f)}{W_f} \quad . \tag{5}$$

Equation 5 indicates that the flux change is independent of pitch angle, and hence, from the assumed isotropy at B_i, we see that the fluxes will be isotropic within the cone defined by equation 4. In addition, the fluxes will be increased by the energy ratio, W_f/W_i.

DISCUSSION

In an attempt to explain the enhanced probability of observing field-aligned precipitation at high altitudes during the winter months, we now examine the relationship between seasonal ionospheric density variations and parallel electric fields. The ionospheric instabilities described by Kindel and Kennel (1971), which give rise to anomalous resistivities resulting in the creation of parallel electric fields, are dependent on

density. Ionospheric density at high altitudes is appreciably greater under sunlit, summer conditions than during winter conditions, due to thermal expansion of the ionosphere. Thus, parallel electric fields can exist at lower altitudes in winter than in summer.

Consider for example a possible summer situation. When the particle flux exceeds the critical instability value, anomalous resistivity will occur, creating a region of parallel electric field as indicated schematically in the top portion of Figure 5. Since the entire region of $E_{\parallel}$ exists at altitudes greater than satellite apogee, only those electrons initially in the shaded region where the potential is ~ 2.3 kV will be detected as field-aligned 2.3 keV electrons at any satellite altitude from apogee to perigee. In this $E_{\parallel}$ configuration, approximately equal numbers of field-aligned 2.3 keV electrons would be detected at altitudes < 500 km and > 800 km, which is the situation indicated for the summer months in Table 2.

In the winter months, the parallel electric field region can occur at considerably lower altitudes than in summer. Winter upper ionospheric densities are much less than summer values, especially at nighttime, and consequently, anomalous resistivities can be triggered at much lower altitudes by currents of similar intensities. Consider the situation illustrated in the lower part of Figure 5, where a portion of the electric field region extends to altitudes below 900 km. Under this situation, almost all of the (initially cold) electrons would be accelerated to the full value of the potential, exiting the lower portion of the electric field region with energies greater than 2.3 keV. However, if the satellite-borne detectors should pass through the lower part of the $E_{\parallel}$

region, say at altitudes between 800 km and 900 km, then, depending on the maximum potential of the electric field region and its upper altitude, particles with small pitch angles, not accelerated through the full potential, could be measured within the bandpass of the 2.3 keV near-0^{o} pitch angle detector. Hence, under these ideal conditions, the probability of observing field-aligned 2.3 keV electrons would be much greater at altitudes > 800 km than at altitudes < 500 km.

In either the summer or winter field configurations, the electric field strengths necessary to perform the acceleration are of the order of several millivolts per meter. Parallel electric field strengths of about 10 mV/m have been reported by Mozer and Fahleson (1970).

CONCLUSIONS

The increased probability of observing high altitude field-aligned electrons during the winter months argues in support of the Kindel and Kennel theory of electrostatic-wave instabilities resulting in localized parallel electric fields in the ionosphere, which can serve as a mechanism for producing field-aligned particle precipitation. Since this mechanism is seasonally dependent, while other processes further out in the magnetosphere which might be associated with field-aligned precipitation are not seasonally varying phenomena, it seems reasonable to conclude that field-aligned electron precipitation is associated with fairly localized parallel electric fields.

ACKNOWLEDGMENTS

I gratefully acknowledge the many fruitful suggestions and constructive criticisms offered by Dr. R. A. Hoffman. Beneficial discussions with Drs. J. L. Burch and K. Maeda were of great assistance in helping to formulate the proposed electric field acceleration mechanism. Much of this work was based on a dissertation submitted in partial fulfillment of the requirements for the Ph.D. degree at the Catholic University of America, 1972.

REFERENCES

Ackerson, K. L., and L. A. Frank, Correlated satellite measurements of low-energy electron precipitation and ground-based observations of a visible auroral arc, J. Geophys. Res., 77, 1128-1136, 1972.

Berko, F. W., Distributions and characteristics of high-latitude field-aligned electron precipitation, submitted to J. Geophys. Res., 1972.

Chamberlain, J. W., Electric acceleration of auroral particles, Rev. Geophys., 7, 461-482, 1969.

Choy, L. W., R. L. Arnoldy, W. Potter, P. Kintner, and L. J. Cahill, Jr., Field-aligned particle currents near an auroral arc, J. Geophys. Res., 76, 8279-8298, 1971.

Cloutier, P. A., H. R. Anderson, R. J. Park, R. R. Vondrak, R. J. Spiger, and B. R. Sandel, Detection of geomagnetically aligned currents associated with an auroral arc, J. Geophys. Res., 75, 2595-2600, 1970.

Coroniti, F. V., and C. F. Kennel, Polarization of the auroral electrojet, J. Geophys. Res., 77, 2835-2850, 1972.

Fermi, E., Nuclear Physics, p. 37, University of Chicago Press, Chicago, 1950.

Haerendel, G., P. C. Hedgecock, and S.-I. Akasofu, Evidence for magnetic field aligned currents during the substorms of March 18, 1969, J. Geophys. Res., 76, 2382-2395, 1971.

Hanson, W. B., Structure of the ionosphere, in Satellite Environment Handbook, ed. F. S. Johnson, pp. 40-47, Stanford University Press, Stanford, Cal., 1965.

Hoffman, R. A., and D. S. Evans, OGO-4 auroral particles experiment and calibrations, preprint X-611-67-632, GSFC, Greenbelt, Md., 1967.

Hoffman, R. A., and D. S. Evans, Field-aligned electron bursts at high latitudes observed by OGO 4, J. Geophys. Res., 73, 6201-6214, 1968.

Kindel, J. M., and C. F. Kennel, Topside current instabilities, J. Geophys. Res., 76, 3055-3078, 1971.

Mozer, F. S., and U. V. Fahleson, Parallel and perpendicular electric fields in an aurora, Planet. Space Sci., 18, 1563-1571, 1970.

Roederer, J. G., On the adiabatic motion of energetic particles in a model magnetosphere, J. Geophys. Res., 72, 981-992, 1967.

Taylor, H. A., Jr., J. M. Grebowsky, and W. J. Walsh, Structured variations of the plasmapause: Evidence of a corotating plasma tail, J. Geophys. Res., 76, 6806-6814, 1971.

Whalen, B. A., and I. B. McDiarmid, Observations of magnetic-field-aligned auroral-electron precipitation, J. Geophys. Res., 77, 191-202, 1972.

Zmuda, A. J., J. H. Martin, and F. T. Heuring, Transverse magnetic disturbances at 1100 kilometers in the auroral region, J. Geophys. Res., 71, 5033-5054, 1966.

Zmuda, A. J., F. T. Heuring, and J. H. Martin, Dayside magnetic disturbances at 1100 km in the auroral oval, J. Geophys. Res., 72, 1115-1117, 1967.

Zmuda, A. J., J. C. Armstrong, and F. T. Heuring, Characteristics of transverse magnetic disturbances observed at 1100 kilometers in the auroral oval, J. Geophys. Res., 75, 4757-4762, 1970.

FIGURE CAPTIONS

Figure 1. Percent of all field-aligned events per hour UT considering events at all local times and invariant latitudes (light line); considering only events in the interval $67.5^{o} \leq \Lambda \leq 75^{o}$ and 22 hours $\leq$ MLT $\leq$ 01 hours (heavy line).

Figure 2. Percent of all field-aligned events per 3 hours UT for the winter months (solid line) and summer months (dashed line).

Figure 3. Probability of precipitation being field-aligned as a function of altitude for winter and summer, considering data collected at all local times.

Figure 4. Probability of precipitation being field-aligned as a function of altitude for winter and summer, considering data collected in the 22 hours to 01 hour MLT interval.

Figure 5. Schematic representation of two possible parallel electric field configurations: top-probable summer, fully sunlit situation; bottom-possible winter, nighttime situation.

SEASONAL DIFFERENCES IN FIELD-ALIGNED PRECIPITATION FREQUENCY

SEASON	PERCENT OF ALL PRECIPITATION EVENTS	PERCENT OF PRECIPITATION EVENTS IN MLT INTERVAL 22 HOURS-01 HOURS	NUMBER OF FIELD-ALIGNED EVENTS	PERCENT OF ALL FIELD-ALIGNED EVENTS NORMALIZED TO EVEN SEASONAL SAMPLING
Winter	9.54	24.33	1260	39.44
Spring	16.05	11.53	1352	25.16
Summer	50.17	12.65	2122	12.63
Autumn	24.24	11.34	1848	22.77

TABLE 1

ALTITUDE VARIATION OF FIELD-ALIGNED PRECIPITATION

SEASON	ALTITUDE RANGE (km)	PERCENT OF ALL EVENTS IN THAT SEASON	PERCENT OF ALL FIELD-ALIGNED EVENTS IN THAT SEASON	PROBABILITY OF EVENT BEING FIELD-ALIGNED IN THAT ALTITUDE RANGE IN THAT SEASON
Winter	< 500	34.6%	19.8%	2.85%
	> 800	17.6	38.5	10.91
Spring	< 600	22.5	24.3	2.67
	> 800	25.7	38.4	3.70
Summer	< 500	12.2	24.5	2.47
	> 800	14.5	25.8	2.19
Autumn	< 500	57.0	22.3	0.60
	> 800	9.8	26.4	4.14
All Seasons	< 500	22.7	21.1	1.72
	> 800	15.7	31.9	3.79

TABLE 2

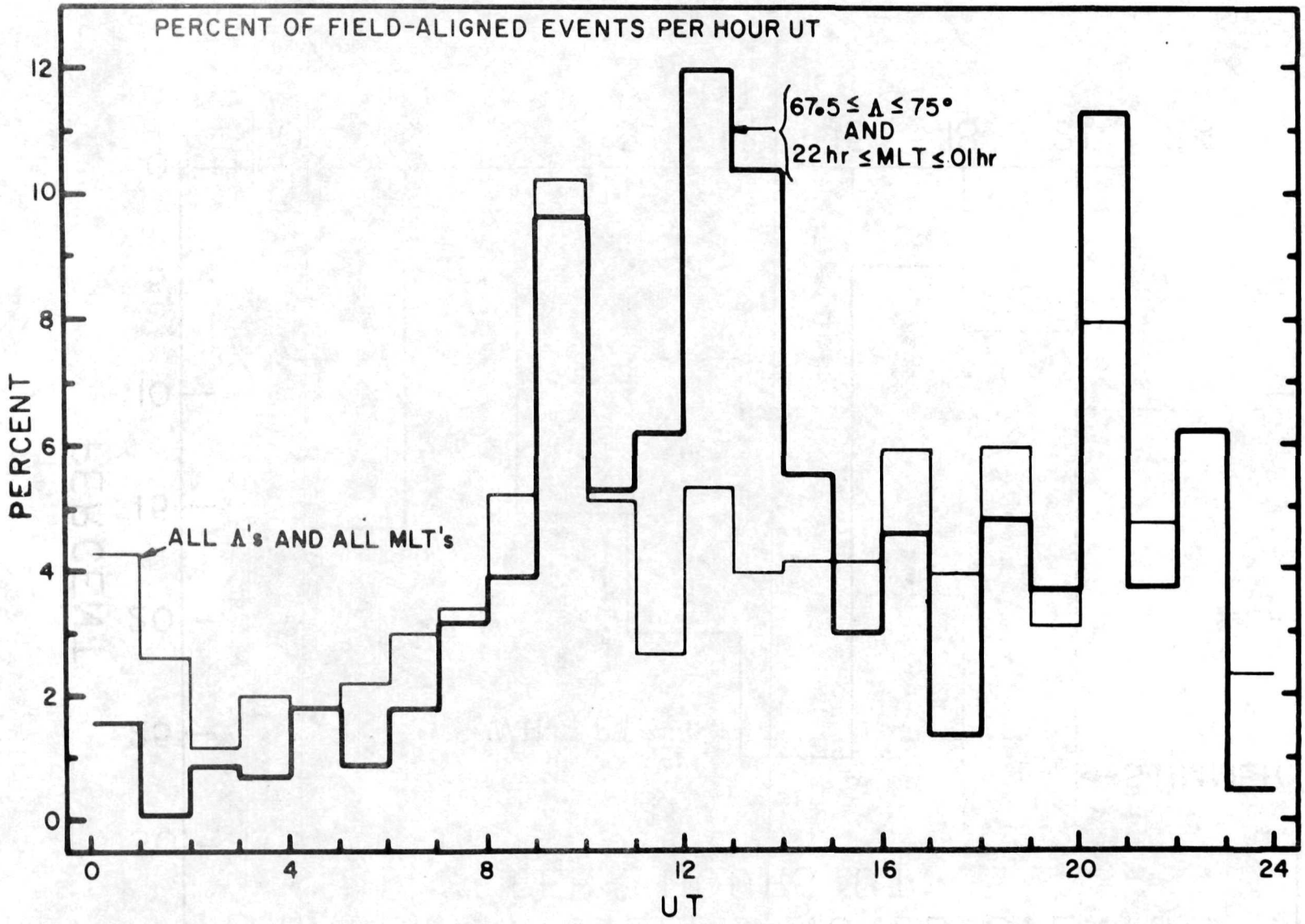
PERCENT OF FIELD-ALIGNED EVENTS PER HOUR UT
67.5 ≤ Λ ≤ 75°
AND
22 hr ≤ MLT ≤ 01 hr
ALL Λ's AND ALL MLT's
PERCENT
UT
0
2
4
6
8
10
12
0
4
8
12
16
20
24

FIGURE 1

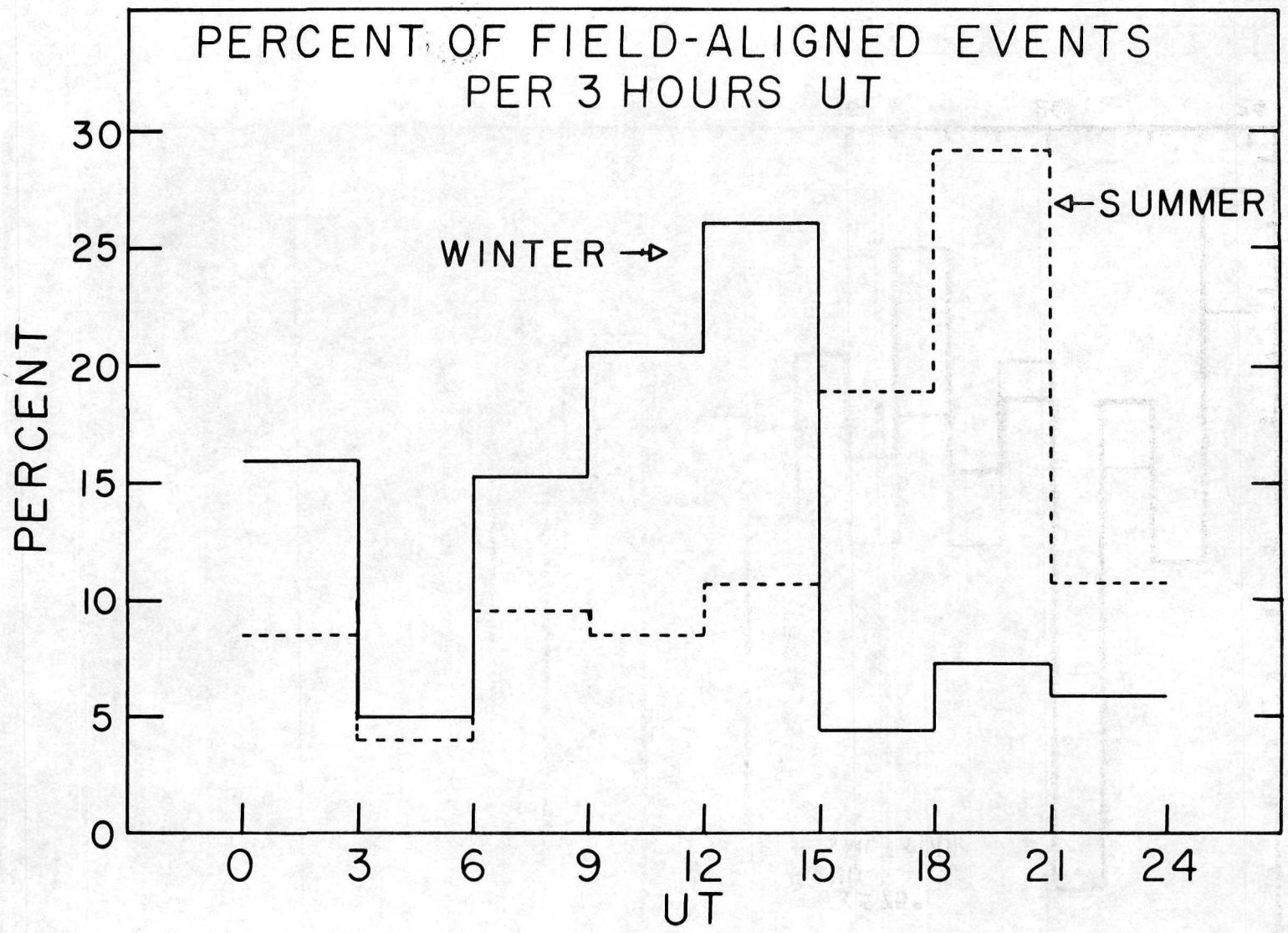
PERCENT OF FIELD-ALIGNED EVENTS
PER 3 HOURS UT
PERCENT
30
25
20
15
10
5
0
WINTER
SUMMER
0
3
6
9
12
15
18
21
24
UT

FIGURE 2

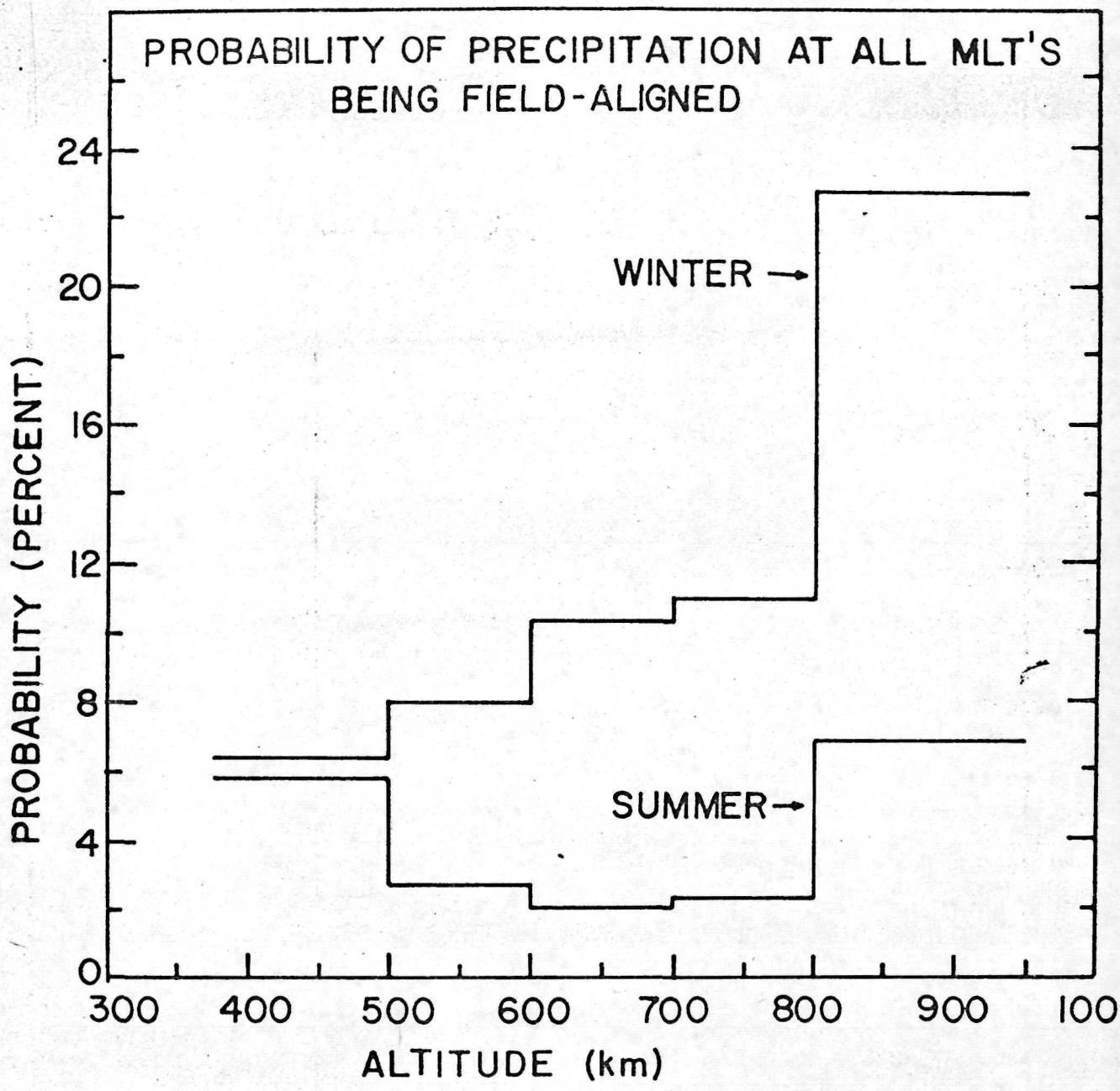
PROBABILITY OF PRECIPITATION AT ALL MLT'S BEING FIELD-ALIGNED
PROBABILITY (PERCENT)
0
4
8
12
16
20
24
WINTER
SUMMER
300
400
500
600
700
800
900
1000
ALTITUDE (km)

FIGURE 3

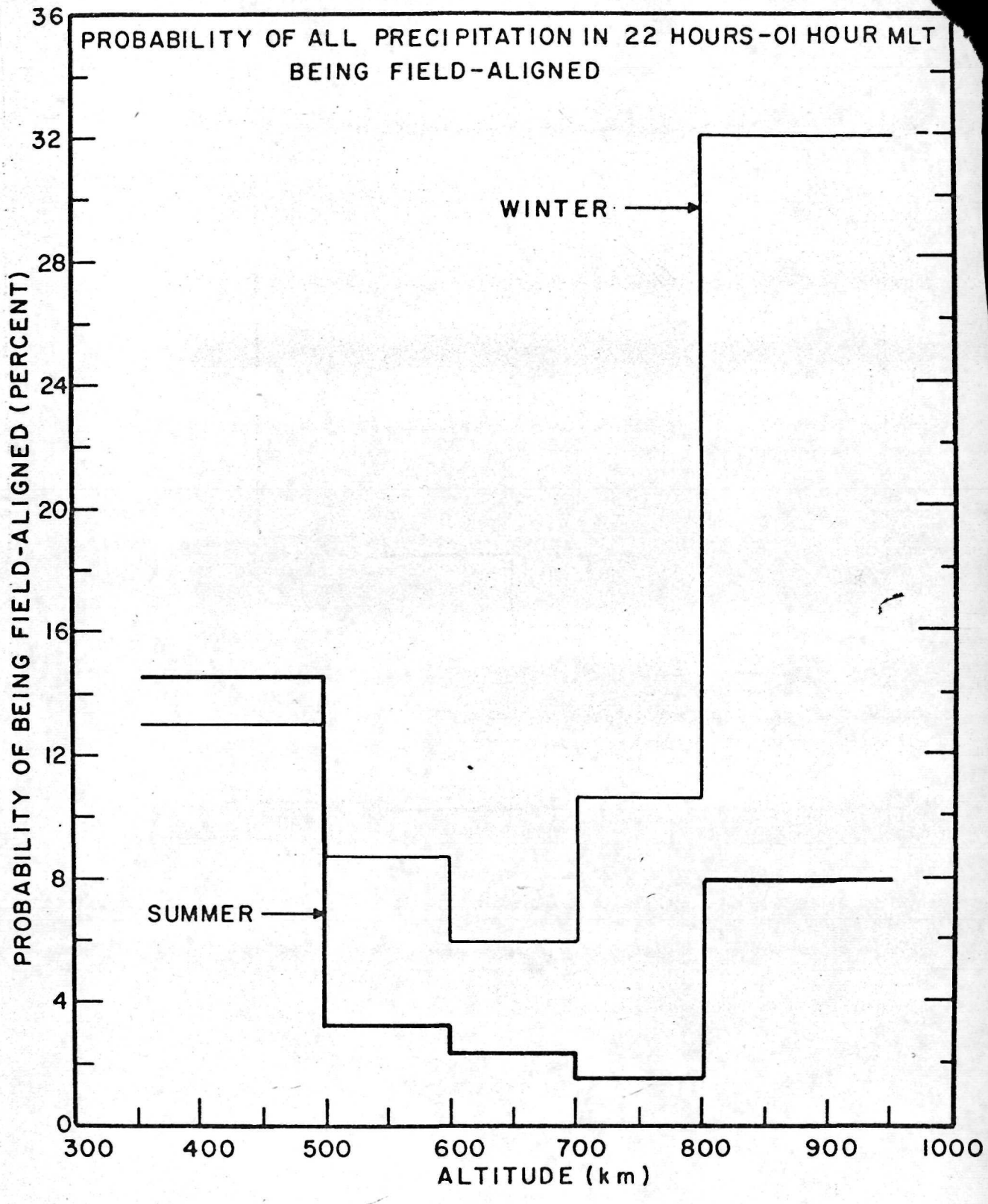
PROBABILITY OF ALL PRECIPITATION IN 22 HOURS-01 HOUR MLT BEING FIELD-ALIGNED
WINTER
SUMMER
PROBABILITY OF BEING FIELD-ALIGNED (PERCENT)
ALTITUDE (km)
0
4
8
12
16
20
24
28
32
36
300
400
500
600
700
800
900
1000

FIGURE 4

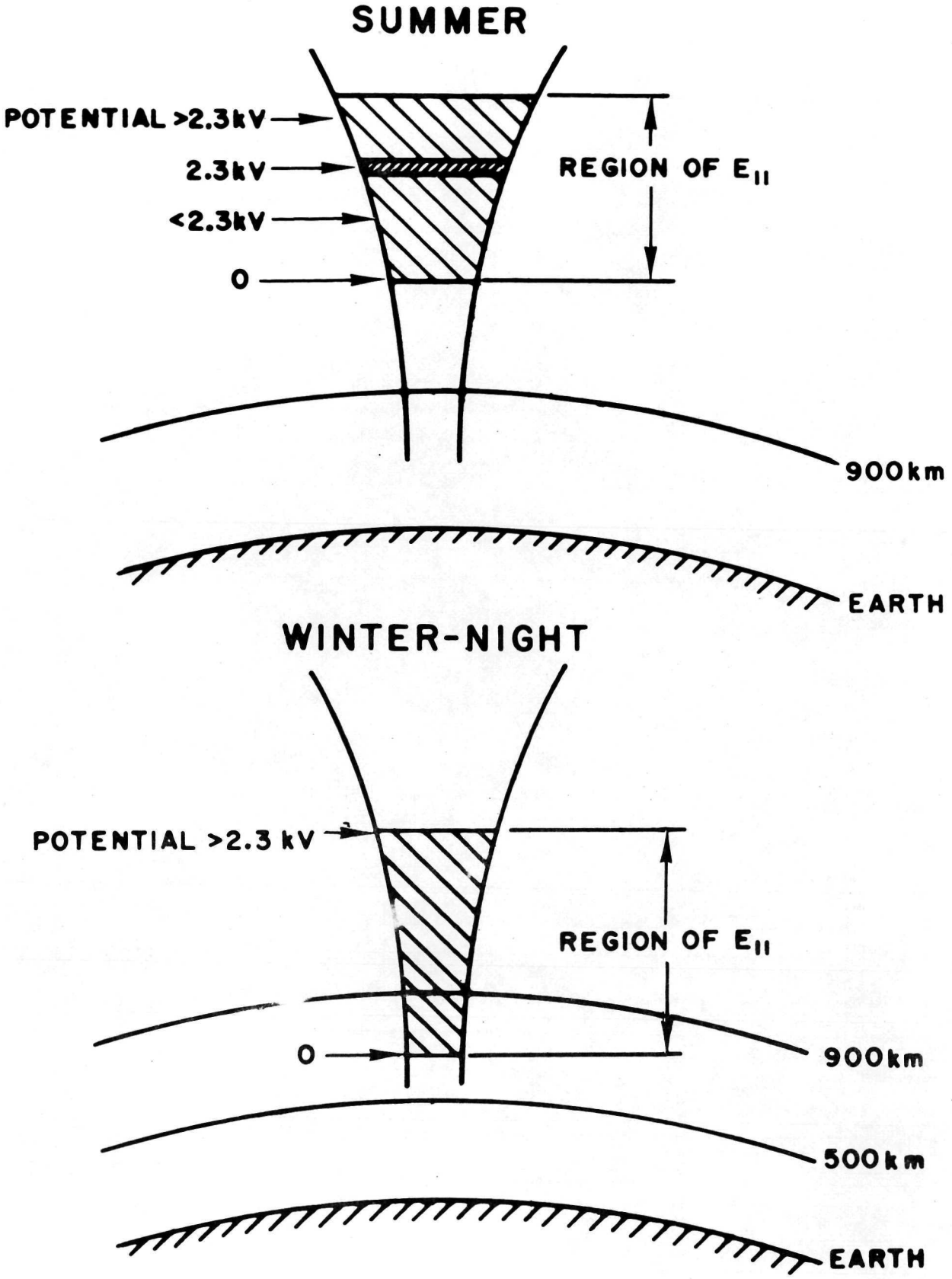
SUMMER
POTENTIAL >2.3kV
2.3kV
<2.3kV
0
REGION OF E||
900km
EARTH
WINTER-NIGHT
POTENTIAL >2.3 kV
REGION OF E||
0
900km
500km
EARTH

FIGURE 5